

Adaptive Nonlinear Control of a Bicopter with Unknown Dynamics

Jhon Manuel Portella Delgado and Ankit Goel

Abstract—This paper presents an adaptive input-output linearization controller with a finite-time convergent parameter estimator for the multicopter trajectory following problem. The controller is constructed by augmenting the input-output linearizing controller based on a dynamically extended multicopter model with a parameter estimator with finite-time convergence properties. Unlike control systems based on the time separation principle to separate the translational and rotational dynamics, the proposed technique is applied to design a controller for the full nonlinear dynamics of the system to obtain desired transient performance. The proposed controller is validated in simulation for a smooth and nonsmooth trajectory-following problem.

keywords: feedback linearization, finite-time estimation, bicopter.

I. INTRODUCTION

Multicopter UAVs have found great success as an inexpensive tool in several engineering applications such as precision agriculture [1], environmental survey [2], [3], construction management [4] and load transportation [5]. However, the low cost of building and operating such platforms fuels novel configurations and designs. Furthermore, the intended operating envelope continually expands as the novel designs are used in novel applications. Thus, due to nonlinear, often time-varying, and unmodeled dynamics, unknown and uncertain operating environments, and fast development cycles of novel configurations, multicopter control remains a challenging control problem.

Several control techniques have been applied to design control systems for multicopters [6]–[8]. However, these techniques often require an accurate plant model and, thus, are susceptible to unmodeled dynamics, and physical model parameter uncertainty [9], [10]. Several adaptive control techniques have been applied to address the problem of unmodeled, unknown, and uncertain dynamics, such as model reference adaptive control [11], [12], L1 adaptive control [13], adaptive sliding mode control [14]–[16], retrospective cost adaptive control [17], [18].

Jhon Manuel Portella Delgado is a graduate student in the Department of Mechanical Engineering, University of Maryland, Baltimore County, 1000 Hilltop Circle, Baltimore, MD 21250. jportell@umbc.edu

Ankit Goel is an Assistant Professor in the Department of Mechanical Engineering, University of Maryland, Baltimore County, 1000 Hilltop Circle, Baltimore, MD 21250. ankgoel@umbc.edu

The dynamics of a multicopter consist of coupled translational and rotational dynamics, resulting in 12th-order nonlinear dynamics. The *state-of-the-art* control architectures decompose the nonlinear dynamics into simpler subsystem dynamics [19]. The state-of-the-art control systems consist of cascaded controllers in a multiloop architecture. The outer loop, whose output is the thrust vector, controls the translational dynamics, and the inner loop, whose output is the torque vector, controls the rotational dynamics. The force and torque control signals are then realized by the propellers of the multicopter using control allocation algorithms.

Although controllers with theoretical performance guarantees can be designed and implemented for each loop in a cascaded control system, the performance of the closed-loop system can not be guaranteed. In fact, the cascaded control systems are based on the time separation principle to justify the cascaded loop architecture, which applies to the case where each successive loop is significantly faster than the previous loop. This crucial assumption allows the coupled dynamics to be decoupled and is used to design simpler controllers for each loop. However, as is well known, the entire control system fails if any loop fails. Since the controllers in each loop are often manually tuned, such cascaded control systems are highly susceptible to failure.

In this paper, we thus consider the problem of designing an adaptive control system for the fully coupled nonlinear dynamics of a multicopter system. To simplify the presentation of the controller design technique, we consider a bicopter system, which retains the coupled nonlinear dynamics of a quadcopter system, but is modeled by a 6th-order nonlinear system instead of a 12th-order nonlinear system [20], [21].

The controller proposed in this work is based on the input-output linearization (IOL) technique [22]–[24]. To avoid the singularity of the resulting nonlinear input map by applying the IOL technique to the 6th-order nonlinear system, we first dynamically extend the system to design a linearizing controller [25]. A simple static feedback controller is then designed to obtain desired transient characteristics and follow a desired trajectory. Finally, we design an adaptive parameter estimator with finite-time convergence property to quickly estimate the uncertain parameters of the nonlinear dynamics. The contributions of this paper are thus 1) the design of a linearizing controller for the fully nonlinear extended

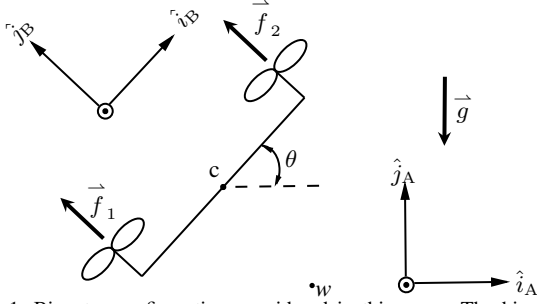


Fig. 1: Bicopter configuration considered in this paper. The bicopter is constrained to the $\hat{i}_A - \hat{j}_A$ plane and rotates about the \hat{k}_A axis of the inertial frame F_A .

bicopter system without decoupling the nonlinear system into simpler subsystems, 2) the adaptive extension of the proposed controller with a finite-time convergent parameter estimator, and 3) validation of the proposed controller in a smooth and a nonsmooth trajectory following problem.

The paper is organized as follows. Section II derives the equation of motion of the bicopter system. Section III presents the adaptive input-output linearizing controller for the extended bicopter system. Section IV presents simulation results to validate the control system proposed in this work. Finally, the paper concludes with a discussion of results and future research directions in section V.

II. BICOPTER DYNAMICS

This section derives the equation of motion of a bicopter system considered in this paper. Let F_A be an inertial frame and let F_B be a frame fixed to the bicopter \mathcal{B} as shown in Figure 1. Note that F_B is obtained by rotating it about the \hat{k}_A axis of F_A by θ , and thus

$$F_A \xrightarrow{\theta} F_B. \quad (1)$$

Letting c denote the center of mass of the bicopter and w denote a fixed point on Earth, it follows from Newton's second law that

$$m \overset{A \bullet \bullet}{\vec{r}}_{c/w} = m \vec{g} + \vec{f}, \quad (2)$$

where m is the mass of the bicopter, \vec{g} is the acceleration due to gravity, and \vec{f} is the total force applied by the propellers to the bicopter. Letting $\vec{f}_1 = f_1 \hat{j}_B$ and $\vec{f}_3 = f_3 \hat{j}_B$ denote the forces applied by the two propellers, it follows that $\vec{f} = f_1 \hat{j}_B + f_2 \hat{j}_B$. Writing $\vec{r}_{c/w} = r_1 \hat{i}_A + r_2 \hat{j}_A$ yields

$$m \ddot{r}_1 = -(f_1 + f_2) \sin \theta, \quad (3)$$

$$m \ddot{r}_2 = (f_1 + f_2) \cos \theta - mg. \quad (4)$$

Next, it follows from Euler's equation that

$$\vec{J}_{B/c} \overset{A \bullet \bullet}{\vec{\omega}}_{B/A} = \vec{M}_{B/c}. \quad (5)$$

Note that $\vec{J}_{B/c} \overset{A \bullet \bullet}{\vec{\omega}}_{B/A} = J \ddot{\theta} \hat{k}_B$ and $\vec{M}_{B/c} = \ell(f_2 - f_1) \hat{k}_B$, where ℓ is the length of the bicopter arm, and thus it follows from (5) that

$$J \ddot{\theta} = \ell(f_2 - f_1). \quad (6)$$

The equations of motion of the bicopter, given by (3), (4), and (6), can be written in state-space form as

$$\dot{x} = f(x, u), \quad (7)$$

where

$$x \triangleq [r_1 \quad r_2 \quad \theta \quad \dot{r}_1 \quad \dot{r}_2 \quad \dot{\theta}]^T, \quad (8)$$

$$u \triangleq [f_1 + f_2 \quad \ell(f_2 - f_1)]^T, \quad (9)$$

and

$$f(x, u) \triangleq \begin{bmatrix} x_4 \\ x_5 \\ x_6 \\ \frac{-u_1 \sin x_3}{m} \\ -g + \frac{u_1 \cos x_3}{m} \\ \frac{u_2}{J} \end{bmatrix}. \quad (10)$$

III. ADAPTIVE DYNAMIC INPUT-OUTPUT LINEARIZING CONTROL

This section develops an adaptive, dynamic, input-output linearizing (A-DIOL) controller for the bicopter with unknown dynamics to follow a desired trajectory. The A-DIOL controller is designed by first dynamically extending the system and designing an input-output linearizing controller for the extended system and then augmenting the controller with a finite-time convergent parameter estimator. Note that, in the bicopter system, dynamic extension is necessary to avoid the singularity of the input map that needs inversion to design the linearizing controller. We dynamically extend The bicopter system is dynamically extended by defining

$$w \triangleq \begin{bmatrix} \ddot{u}_1 \\ u_2 \end{bmatrix}, \quad \chi \triangleq \begin{bmatrix} x \\ u_1 \\ \dot{u}_1 \end{bmatrix}, \quad (11)$$

which yields the dynamically extended system

$$\dot{\chi} = F(\chi) + G(\chi)w, \quad (12)$$

where

$$F(\chi) \triangleq \begin{bmatrix} \chi_4 \\ \chi_5 \\ \chi_6 \\ -\frac{\sin \chi_3}{m} \chi_7 \\ -g + \frac{\cos \chi_3}{m} \chi_7 \\ 0 \\ \chi_8 \\ 0 \end{bmatrix}, \quad G(\chi) \begin{bmatrix} 0 & 0 \\ 0 & 0 \\ 0 & 0 \\ 0 & 0 \\ 0 & 0 \\ 0 & \frac{1}{J} \\ 1 & 0 \end{bmatrix}. \quad (13)$$

To design a control law that linearizes the dynamics from the input to the position output of the bi-copter, we consider the output

$$y = H(\chi) = \begin{bmatrix} \chi_1 \\ \chi_2 \end{bmatrix} = \begin{bmatrix} x_1 \\ x_2 \end{bmatrix} = \begin{bmatrix} r_1 \\ r_2 \end{bmatrix}. \quad (14)$$

Note that the relative degrees ρ_1 and ρ_2 of y_1 and y_2 are 4, and thus the total relative degree ρ of the extended system is 8. Since $\rho = 8$ is equal to the dimension of the extended system state χ , there are no zero dynamics. In this paper, we use the input-output linearization technique presented in [26, p. 517], [27] to design the control law. The linearizing control law is thus

$$w = -\beta(\chi)^{-1}(\alpha(\chi) - v), \quad (15)$$

where

$$\begin{aligned} \alpha(\chi) &= \begin{bmatrix} L_F^4 H_1(\chi) \\ L_F^4 H_2(\chi) \end{bmatrix} \\ &= \begin{bmatrix} \frac{\chi_6 (2\chi_8 \cos(\chi_3) - \chi_6 \chi_7 \sin(\chi_3))}{-\chi_6 (2\chi_8 \sin(\chi_3) + \chi_6 \chi_7 \cos(\chi_3))} \\ m \end{bmatrix}, \end{aligned} \quad (16)$$

$$\beta(\chi) \triangleq \begin{bmatrix} L_G L_F^3 H_1(\chi) \\ L_G L_F^3 H_2(\chi) \end{bmatrix} = \begin{bmatrix} -\frac{\sin \chi_3}{m} & -\frac{\cos \chi_3 \chi_7}{m J} \\ \frac{\cos \chi_3}{m} & -\frac{\sin \chi_3 \chi_7}{m J} \end{bmatrix}, \quad (17)$$

and, assuming $\chi_7 = u_1 \neq 0$, which is a reasonable assumption in multicopter control,

$$\beta^{-1}(\chi) = \begin{bmatrix} -\frac{m \sin(\chi_3)}{J m \cos(\chi_3)} & \frac{m \cos(\chi_3)}{J m \sin(\chi_3)} \\ -\frac{1}{\chi_7} & -\frac{1}{\chi_7} \end{bmatrix}. \quad (18)$$

The linearizing controller (15) yields the linearized dynamics

$$\dot{\xi} = A_\xi \xi + B_\xi v, \quad (19)$$

where the state ξ of the transformed system is

$$\xi \triangleq \begin{bmatrix} H_1(\chi) \\ \vdots \\ L_F H_1^{\rho_1-1}(\chi) \\ H_2(\chi) \\ \vdots \\ L_F H_2^{\rho_2-1}(\chi) \end{bmatrix} = \begin{bmatrix} \chi_1 \\ \chi_4 \\ -\frac{\sin(\chi_3)}{m} \chi_7 \\ -\frac{\cos(\chi_3)}{m} \chi_7 \chi_6 - \frac{\sin(\chi_3)}{m} \chi_8 \\ \chi_2 \\ \chi_5 \\ -g + \frac{\cos(\chi_3)}{m} \chi_7 \\ -\frac{\sin(\chi_3)}{m} \chi_7 \chi_6 + \frac{\cos \chi_3}{m} \chi_8 \end{bmatrix}, \quad (20)$$

and the dynamics and input matrices of the linearized system are

$$A_\xi \triangleq \begin{bmatrix} 0 & 1 & 0 & 0 & 0 & 0 & 0 & 0 \\ 0 & 0 & 1 & 0 & 0 & 0 & 0 & 0 \\ 0 & 0 & 0 & 1 & 0 & 0 & 0 & 0 \\ 0 & 0 & 0 & 0 & 0 & 0 & 0 & 0 \\ 0 & 0 & 0 & 0 & 0 & 1 & 0 & 0 \\ 0 & 0 & 0 & 0 & 0 & 0 & 1 & 0 \\ 0 & 0 & 0 & 0 & 0 & 0 & 0 & 1 \\ 0 & 0 & 0 & 0 & 0 & 0 & 0 & 0 \end{bmatrix}, B_\xi \triangleq \begin{bmatrix} 0 & 0 \\ 0 & 0 \\ 0 & 0 \\ 1 & 0 \\ 0 & 0 \\ 0 & 0 \\ 0 & 0 \\ 0 & 1 \end{bmatrix}. \quad (21)$$

To track a desired state trajectory ξ_d , we use the control law

$$v = K(\xi - \xi_d) + B_\xi^T \dot{\xi}_d, \quad (22)$$

where the gain matrix K is computed using the eigenvalue placement technique to place the eigenvalues of the closed-loop error dynamics

$$\dot{e} = (A_\xi + B_\xi K)e, \quad (23)$$

where $e \triangleq \xi - \xi_d$, at a desired location. The desired eigenvalues of the error dynamics are chosen to satisfy user-specified transient characteristics. Note that

$$B_\xi^T \dot{\xi}_d = \begin{bmatrix} \dot{\xi}_{d4} \\ \dot{\xi}_{d8} \end{bmatrix} = \begin{bmatrix} y_{d1}^{(4)} \\ y_{d2}^{(4)} \end{bmatrix}, \quad (24)$$

which is assumed to be available for smooth trajectories. For nonsmooth trajectories, we set $B_\xi^T \dot{\xi}_d = 0$ if $\dot{\xi}_d$ is undefined. As shown in Section IV, this modification does not negatively impact the closed-loop response.

The linearizing control law (15) requires the precise knowledge of the mass m and the inertia J of the bi-copter. However, since these physical parameters are not typically precisely known or are often time-varying, we use an online parameter estimator with finite-time convergence property to estimate them.

To estimate the unknown parameters, we use the bi-copter system (7) to formulate a linear regressor equation as shown below. In particular, we write (7) as

$$\dot{x} - \Psi(x) = \Phi(x, u)\Theta, \quad (25)$$

where

$$\Psi(x) \triangleq \begin{bmatrix} x_4 \\ x_5 \\ x_6 \\ 0 \\ -g \\ 0 \end{bmatrix}, \Phi(x, u) \triangleq \begin{bmatrix} 0 & 0 \\ 0 & 0 \\ 0 & 0 \\ -\sin(x_3)u_1 & 0 \\ \cos(x_3)u_1 & 0 \\ 0 & u_2 \end{bmatrix}, \quad (26)$$

and

$$\Theta \triangleq \begin{bmatrix} m^{-1} \\ J^{-1} \end{bmatrix}. \quad (27)$$

Since x and u are assumed to be known, the signals Ψ and Φ can be computed online. However, \dot{x} is unknown. To avoid the requirement of \dot{x} , we filter (25) with an asymptotically stable filter $R(s)$ to obtain the linear regressor

$$x_f = \Phi_f \Theta, \quad (28)$$

where

$$x_f \triangleq R(s)(\dot{x} - \Psi(x)), \quad \Phi_f \triangleq R(s)(\Phi(x, u)). \quad (29)$$

Letting $R(s) = \frac{1}{s + \gamma}$, where $\gamma > 0$, yields

$$x_f = \frac{sx}{s + \gamma} - \frac{\Psi(x)}{s + \gamma}, \quad \Phi_f = \frac{\Phi(x, u)}{s + \gamma}. \quad (30)$$

Note that x_f and Φ_f can now be computed online using only the measurements of the state x and the input u .

Finally, we use the estimator

$$\dot{\hat{\Theta}} = -c_1 \frac{\Xi}{\|\Xi\|_2^{1-\alpha_1}} - c_2 \frac{\Xi}{\|\Xi\|_2^{1-\alpha_2}}, \quad (31)$$

where

$$\Xi \triangleq \bar{\Phi} \hat{\Theta} - \bar{X}, \quad (32)$$

$c_1, c_2 > 0$, $0 < \alpha_1 < 1$, and $\alpha_2 > 1$, and

$$\dot{\bar{X}} = -\lambda \bar{X} + \Phi_f^T x_f, \quad (33)$$

$$\dot{\bar{\Phi}} = -\lambda \bar{\Phi} + \Phi_f^T \Phi_f. \quad (34)$$

The positive scalar $\lambda > 0$ is the exponential forgetting factor. The data matrices $\bar{X} \in \mathbb{R}^2$ and $\bar{\Phi} \in \mathbb{R}^{2 \times 2}$ are initialized at zero. Note that the finite-time convergent parameter estimator (31) is constructed by modifying the gradient-based exponentially stable parameter estimator using the finite-time optimization theory presented in [28], [29].

The adaptive control law is thus (15), where α and β are computed with the estimates of m and J given by (31), and v is given by the tracking controller (22).

IV. NUMERICAL SIMULATIONS

This section presents the numerical simulation results obtained by applying the A-DIOL controller to the trajectory following problem for a bicopter. In particular, we use the A-DIOL controller to follow a smooth elliptical trajectory and a nonsmooth trajectory based on a second-order Hilbert curve.

In this work, we assume that the mass of the bicopter is 1 kg and its inertia is 0.05 kgm² to simulate the bicopter dynamics. To obtain a setting time less than 2 second, the eigenvalues of the error dynamics (23) are placed at $(-4.5, -4.0, -5, -5.5, -4.5, -4.0, -5, -5.5)$ using Matlab's `place` routine, which yields $K_1 = K_5 = 495, K_2 = K_6 = 422.75, K_3 = K_7 = 134.75$, and $K_4 = K_8 = 19$. Furthermore, in the parameter

estimator, we set $c_1 = 6, c_2 = 3, \alpha_1 = 0.2, \alpha_2 = 1.2, \lambda = 80$, and $\gamma = 10$. Finally, we set the initial estimate $\hat{\Theta}(0) = [2 \ 10]^T$ in the parameter estimator¹.

A. Elliptical Trajectory

The bicopter is commanded to follow a desired elliptical trajectory given by

$$r_{d1}(t) = 5 \cos(\phi) - 5 \cos(\phi) \cos(\omega t) - 3 \sin(\phi) \sin(\omega t), \\ r_{d2}(t) = 5 \sin(\phi) - 5 \sin(\phi) \cos(\omega t) + 3 \cos(\phi) \sin(\omega t),$$

where $\phi = 45$ deg and $\omega = 1$ rad/s⁻¹. Figure 2 shows the trajectory-following response of the bicopter, where the desired trajectory is shown in black dashes, and the trajectory response is shown in blue. Figures 3a) and b) show the horizontal and vertical position r_1 and r_2 , and Figure 3c) shows the roll angle θ of the bicopter. Figures 4a) and b) show the horizontal and vertical position errors, and Figure 4c) shows the norm of the parameter estimate error $\Theta - \hat{\Theta}$ on a logarithmic scale. Finally, Figure 5 shows the control signals generated by the adaptive control law (15).

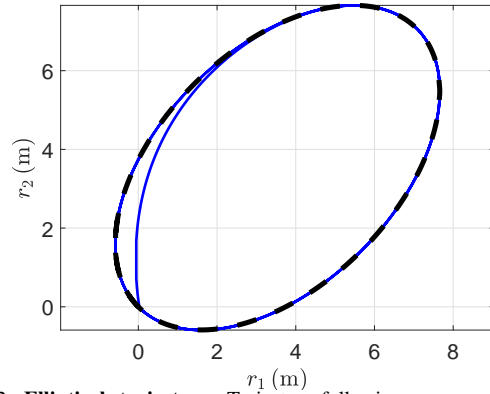


Fig. 2: **Elliptical trajectory.** Trajectory-following response of the bicopter with A-DIOL controller. Note that the output trajectory is in solid blue, and the reference trajectory is in dashed black

B. Second-order Hilbert Curve Trajectory

Next, the bicopter is commanded to follow a non-smooth trajectory constructed using a second-order Hilbert curve. Figure 6 shows the trajectory-following response of the bicopter. The desired trajectory is shown in black dashes and the trajectory response is shown in blue. Figure 7 a) and b) shows the horizontal and vertical position r_1 and r_2 , and c) shows the roll angle θ of the bicopter. Figure 8 a) and b) shows the horizontal and vertical position errors, and c) shows the norm of the parameter estimate error $\Theta - \hat{\Theta}$ on a logarithmic scale. Finally, Figure 9 shows the control signals generated by the adaptive control law (15).

¹<https://github.com/ankgoel18188/A-DIOLbicopter>

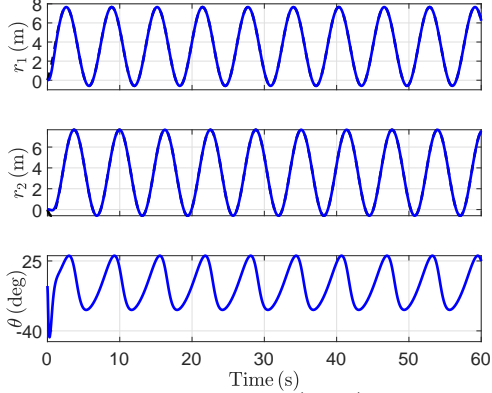


Fig. 3: **Elliptical trajectory.** Positions (r_1, r_2) and the roll angle θ of the bicopter. Note that the desired trajectory is shown in dashed black.

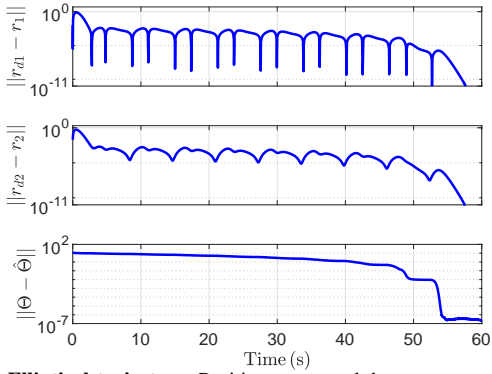


Fig. 4: **Elliptical trajectory.** Position errors and the parameter estimation error on a logarithmic scale. The parameters m and J converge in finite time, as shown by the sharp drop in the parameter estimation error. However, due to numerical precision, the parameter update stops after the error is less than the machine's precision.

These examples show that the bicopter's trajectory converges to the desired trajectory exponentially, and the parameter estimates converge in finite time with the A-DIOL controller in both smooth and nonsmooth trajectory-following problem. Note that due to numerical precision, the parameter update stops after the error is less than the machine's precision.

V. CONCLUSIONS AND FUTURE WORK

This paper presented an adaptive dynamic input-output linearizing controller for the bicopter trajectory-following problem. The adaptive controller was constructed by augmenting the feedback linearization controller with a finite-time convergent parameter estimator. The performance of the proposed controller was validated in numerical simulation of a smooth and a nonsmooth trajectory-following problem. Although the work in this paper does not present a stability analysis of the proposed adaptive controller, numerical simulations confirm that the closed-loop error dynamics is exponentially stable and the parameter estimates converge in finite time.

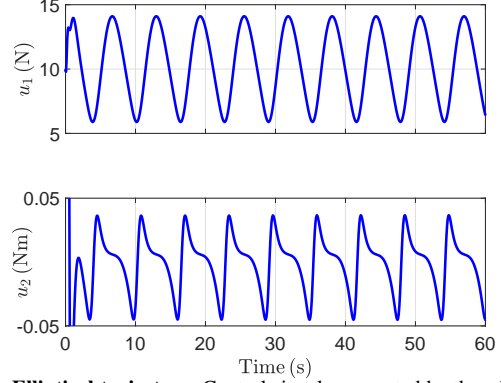


Fig. 5: **Elliptical trajectory.** Control signals computed by the adaptive controller (15).

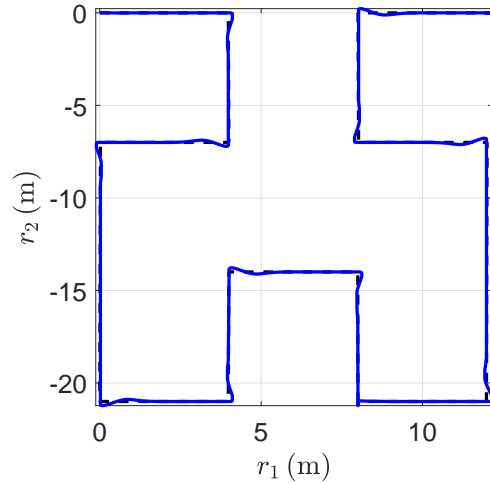


Fig. 6: **Hilbert trajectory.** Trajectory-following response of the bicopter with A-DIOL controller. Note that the output trajectory is in solid blue, and the desired trajectory is in dashed black.

Our future work will focus on relaxing the requirement of full-state feedback by incorporating a finite-time convergent state estimator, characterizing the robustness of the proposed controller to sensor noise, and presenting a rigorous stability analysis of the proposed adaptive control system.

REFERENCES

- [1] A. Mukherjee, S. Misra, and N. S. Raghuvanshi, "A survey of unmanned aerial sensing solutions in precision agriculture," *J. Netw. Comput. Appl.*, vol. 148, p. 102461, 2019.
- [2] A. Lucieer, S. M. d. Jong, and D. Turner, "Mapping landslide displacements using Structure from Motion (SfM) and image correlation of multi-temporal UAV photography," *Prog. Phys. Geogr.*, vol. 38, no. 1, pp. 97–116, 2014.
- [3] V. V. Klemas, "Coastal and environmental remote sensing from unmanned aerial vehicles: An overview," *J. Coast. Res.*, vol. 31, no. 5, pp. 1260–1267, 2015.
- [4] Y. Li and C. Liu, "Applications of multirotor drone technologies in construction management," *Int. J. Constr. Manag.*, vol. 19, no. 5, pp. 401–412, 2019.
- [5] D. K. Villa, A. S. Brandao, and M. Sarcinelli-Filho, "A survey on load transportation using multirotor UAVs," *J. Intell. Robot. Syst.*, vol. 98, pp. 267–296, 2020.

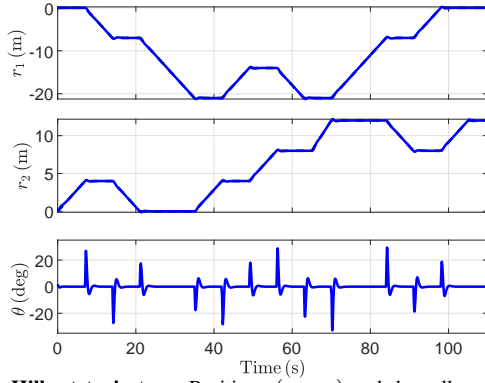


Fig. 7: **Hilbert trajectory**. Positions (r_1, r_2) and the roll angle θ of the bicopter. Note that the desired trajectory is shown in dashed black.

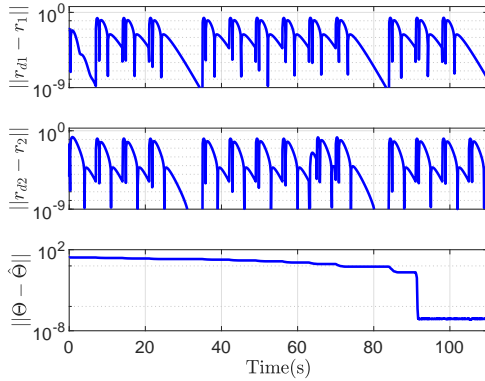


Fig. 8: **Hilbert trajectory**. Position errors and the parameter estimation error on a logarithmic scale. The parameters m and J converge in finite time, as shown by the sharp drop in the parameter estimation error. However, due to numerical accuracy, the parameter update stops after the error is less than the machine's precision.

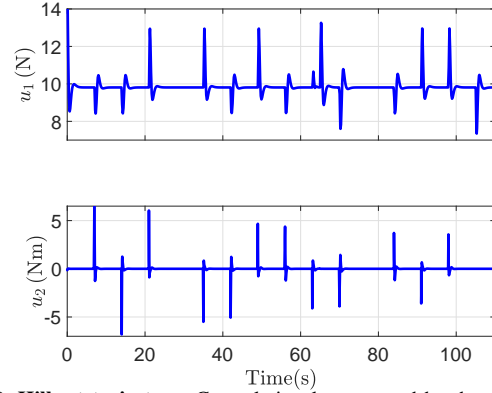


Fig. 9: **Hilbert trajectory**. Control signals computed by the adaptive controller (15).

[6] T. P. Nascimento and M. Saska, "Position and attitude control of multi-rotor aerial vehicles: A survey," *Annu. Rev. Contr.*, vol. 48, pp. 129–146, 2019.

[7] J. A. Marshall, W. Sun, and A. L'Afflito, "A survey of guidance, navigation, and control systems for autonomous multi-rotor small unmanned aerial systems," *Annu. Rev. Contr.*, vol. 52, pp. 390–427, 2021.

[8] P. Castillo, A. Dzul, and R. Lozano, "Real-time stabilization and tracking of a four-rotor mini rotorcraft," *IEEE Trans. Contr. Sys. Tech.*, vol. 12, no. 4, pp. 510–516, 2004.

[9] B. J. Emran and H. Najjaran, "A review of quadrotor: An underactuated mechanical system," *Annu. Rev. Contr.*, vol. 46, pp. 165–180, 2018.

[10] R. Amin, L. Aijun, and S. Shamshirband, "A review of quadrotor UAV: Control methodologies and performance evaluation," *Int. J. Autom. Contr.*, vol. 10, no. 2, pp. 87–103, 2016.

[11] B. Whitehead and S. Bieniawski, "Model reference adaptive control of a quadrotor UAV," in *AIAA Guid. Nav. Contr. Conf. Ex.*, 2010, p. 8148.

[12] Z. T. Dydek, A. M. Annaswamy, and E. Lavretsky, "Adaptive control of quadrotor UAVs: A design trade study with flight evaluations," *IEEE Trans. Contr. Sys. Tech.*, vol. 21, no. 4, pp. 1400–1406, 2012.

[13] Z. Zuo and P. Ru, "Augmented L1 adaptive tracking control of quad-rotor unmanned aircrafts," *IEEE. Trans. Aerosp. Elec. Sys.*, vol. 50, no. 4, pp. 3090–3101, 2014.

[14] T. Espinoza-Fraire, A. Saenz, F. Salas, R. Juarez, and W. Giernacki, "Trajectory tracking with adaptive robust control for quadrotor," *Applied Sciences*, vol. 11, no. 18, p. 8571, 2021.

[15] Z. Wu, S. Cheng, K. A. Ackerman, A. Gahlawat, A. Lakshmanan, P. Zhao, and N. Hovakimyan, "L1 adaptive augmentation for geometric tracking control of quadrotors," in *2022 International Conference on Robotics and Automation (ICRA)*, IEEE, 2022, pp. 1329–1336.

[16] O. Mofid and S. Mobayen, "Adaptive sliding mode control for finite-time stability of quad-rotor UAVs with parametric uncertainties," *ISA trans.*, vol. 72, pp. 1–14, 2018.

[17] A. Goel, J. A. Paredes, H. Dadhaniya, S. A. Ul Islam, A. M. Salim, S. Ravela, and D. Bernstein, "Experimental implementation of an adaptive digital autopilot," in *Proc. Amer. Contr. Conf.*, 2021, pp. 3737–3742.

[18] J. Spencer, J. Lee, J. A. Paredes, A. Goel, and D. Bernstein, "An adaptive PID autotuner for multicopters with experimental results," in *Proc. Int. Conf. Rob. Autom.*, IEEE, 2022, pp. 7846–7853.

[19] PX4 User Guide, *Multicopter Control Architecture*, https://docs.px4.io/main/en/flight_stack/controller_diagram [Online; accessed 26 February 2023].

[20] T. Meinschmidt and H. Aschemann, "Cascaded flatness-based control of a duocopter subject to unknown disturbances," in *2014 19th International Conference on Methods and Models in Automation and Robotics (MMAR)*, IEEE, 2014, pp. 845–850.

[21] T. Meinschmidt, H. Aschemann, and S. S. Butt, "Cascaded backstepping control of a duocopter including disturbance compensation by unscented kalman filtering," in *2014 International Conference on Control, Decision and Information Technologies (CoDIT)*, IEEE, 2014, pp. 315–320.

[22] J.-J. E. Slotine, W. Li, et al., *Applied nonlinear control*, 1. Prentice hall Englewood Cliffs, NJ, 1991, vol. 199.

[23] A. Isidori, *Nonlinear control systems: an introduction*. Springer, 1985.

[24] H. K. Khalil, *Nonlinear control*. Pearson New York, 2015, vol. 406.

[25] L. Triska, J. Portella, and J. Reger, "Dynamic extension for adaptive backstepping control of uncertain pure-feedback systems," *IFAC-PapersOnLine*, vol. 54, no. 14, pp. 307–312, 2021.

[26] H. K. Khalil, *Nonlinear systems; 3rd ed.* Upper Saddle River, NJ: Prentice-Hall, 2002.

[27] J. M. Portella Delgado and A. Goel, "MIMO input-output linearization with applications for longitudinal flight dynamics," *arXiv e-prints*, arXiv:2205, 2022.

[28] K. Garg and D. Panagou, "Fixed-time stable gradient flows: Applications to continuous-time optimization," *IEEE Transactions on Automatic Control*, vol. 66, no. 5, pp. 2002–2015, 2020.

[29] K. Garg and M. Baranwal, "CAPP: Continuous-time accelerated proximal point algorithm for sparse recovery," *IEEE Signal Processing Letters*, vol. 27, pp. 1760–1764, 2020.